PHYSICAL REVIEW A, VOLUME 61, 041601(R)

Imaging of an atomic beam with electrostatic lenses

Heung-Ryoul Noh,* Kazuko Shimizu, and Fujio Shimizu
Institute for Laser Science, University of Electro-Communications, Chofu-shi, Tokyo 182-8585, Japan
(Received 21 September 1999; published 28 February 2000)

The imaging of a neutral atomic beam by electrostatic force has been demonstrated. An ultracold neon atomic beam in the $1s_3[(2p)^5 3s{:}^1P_0]$ state illuminated a transparent object, passed through a set of three electrostatic lenses, and formed the image on a microchannel plate detector with the magnification of unity. Each lens consisted of two parallel cylinders that functioned as a concave lens along one axis and as a convex lens along the other axis. The atomic polarizability of neon in the $1s_3$ state has been also determined to be $2.8(\pm 0.1)\times 10^{-39}$ Fm^2.

PACS number(s): 03.75.Be, 32.80.Pj

A lens is a basic component among various atom optical elements, such as mirrors, beam splitters, and waveguides [1]. Various kinds of interactions have been used to achieve lenses for focusing or imaging of neutral atoms and molecules. A magnetic field has been used for a long time as a tool to manipulate atomic beams [2]. The imaging of an atomic beam with a hexapole magnetic lens was demonstrated recently [3]. A thin-film transparent optics [4,5] is a promising device, because it can produce in principle an arbitrary wave front. It suffers from the loss of flux and the difficulty of eliminating spurious images. A static electric field has been used to manipulate molecules with a permanent dipole moment [6]. For atoms, however, the electrostatic field has been generally considered as useless, because the electric dipole interaction of an atom in a stable state is negative. Atoms are attracted towards a higher field, and it is not possible to make a local maximum of the field in free space. Ketterle and Pritchard [7] have proved that the focusing by a thin lens is not possible by an electric field. The electric-dipole interaction was used in optical [8–12] and microwave [13,14] fields to focus an atomic beam, because an electromagnetic wave can produce both maxima and minima in free space. Especially, the optical field is a flexible tool, because the direction of the deflection can be reversed by changing the sign of the detuning from the atomic resonance. The optical standing wave was used to make a periodic atomic pattern of several tens of nanometers. It is, however, not easy to make a cylindrically symmetric optics. This paper demonstrates that, in spite of the negative interaction, one can construct a cylindrically symmetric imaging optics for atoms with a combination of one-dimensional electrostatic optical components. A similar technique has been known in charged-particle optics [15,16], and a similar idea was used to trap atoms two dimensionally [17]. When the electric field is two dimensional, $E_z=0$, it is not difficult to prove that the Stark potential Φ at a stationary point is either symmetrically repulsive or is a saddle point having equal curvature along two orthogonal principal axes,

$$\Phi(x,y) = -\tfrac{1}{2}\alpha E^2 \approx \Phi_0 - \tfrac{1}{2}k(x^2-y^2), \tag{1}$$

where α is the atomic probability and k is the spring constant.

A lens that produces the potential of Eq. (1) focuses the atomic beam only in the y-z plane but defocuses in the x-z plane. When a composite lens system is used, the situation is different. The atom can be focused two dimensionally, if we use two lens system in which the two lenses have a 90° rotated orientation. The focusing is achieved if the two lenses are oriented so that the atom travels a larger distance from the optical axis when it passes through the convex potential; therefore, it is deflected by a larger angle. The two-lens system, however, cannot produce the image that has equal magnification along the x and y axes. At least three lenses are needed to produce a perfect image that has equal magnification.

We used two parallel cylinders that had a radius of R and were separated by $2d$ as a lens [see Fig. 1(a)]. Then, the spring constant $k=2\alpha V_0^2/(b^2 \sinh^{-1}\sqrt{d/2R})^2$, and $\Phi_0 = -(1/4)kb^2$, where $b=\sqrt{d(d+2R)}$ and $\pm V_0$ is the potential of each cylinder, respectively. When an atom passed through the lens, its transverse position (x,y) and velocity (x',y') develop according to the equations

$$\begin{pmatrix} x \\ x' \end{pmatrix} = M_d(\omega,t)\begin{pmatrix} x_0 \\ x_0' \end{pmatrix} \quad \text{and} \quad \begin{pmatrix} y \\ y' \end{pmatrix} = M_c(\omega,t)\begin{pmatrix} y_0 \\ y_0' \end{pmatrix},$$

where the transfer matrices are

$$M_d(\omega,t) = \begin{pmatrix} \cosh\omega t & \sinh\omega t/\omega \\ \omega\,\sinh\omega t & \cosh\omega t \end{pmatrix},$$
$$M_c = (\omega,t) = \begin{pmatrix} \cos\omega t & \sin\omega t/\omega \\ -\omega\,\sin\omega t & \cos\omega t \end{pmatrix}. \tag{2}$$

Here, t is the transit time of the atom in the lens, the characteristic frequency $\omega=\sqrt{k/m}$, and m is the mass of the atom.

We used three sets of cylinders to obtain circularly symmetric image (see Fig. 2). The combined transfer matrices from the object to the screen [microchannel plate detector (MCP)] in the x-z and y-z planes, M_x and M_y, respectively, are

*Present address: Center for Near-field Atom-Photon Technology, Seoul National University, Seoul 151-742, Korea.

 ©2000 The American Physical Society

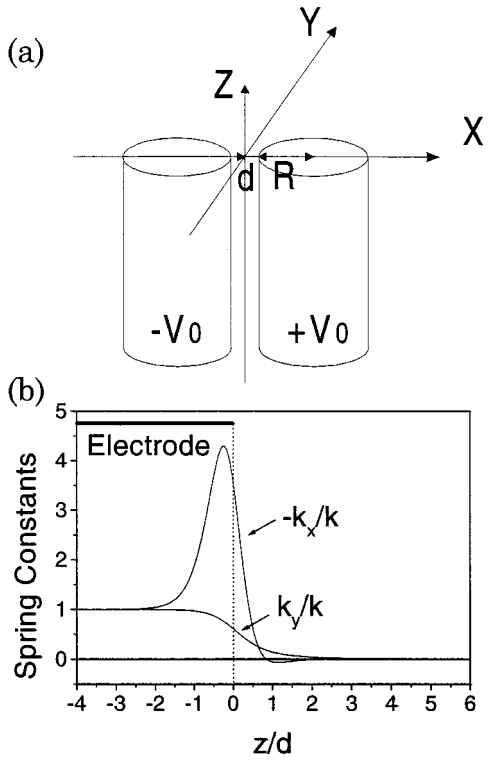

FIG. 1. (a) Scheme of electrostatic atoms lens. (b) The spring constants k_z and k_y as functions of z.

$$M_x = M(t_d)M_d(\omega_3,T_3)M(t_c)M_c(\omega_2,T_2)M(t_b) \times M_d(\omega_1,T_1)M(t_a), \tag{3}$$

$$M_y = M(t_d)M_c(\omega_3,T_3)M(t_c)M_d(\omega_2,T_2)M(t_b) \times M_c(\omega_1,T_1)M(t_a),$$

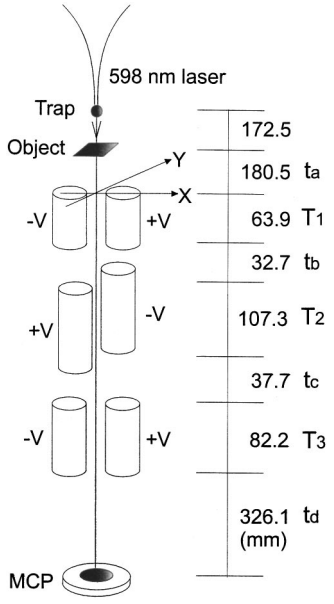

FIG. 2. Experimental setup. Times; $t_a = t_d = 80.7$ ms, $t_b = t_c = 11.2$ ms, $T_1 = T_3 = 23.3$ ms, $T_2 = 34.2$ ms.

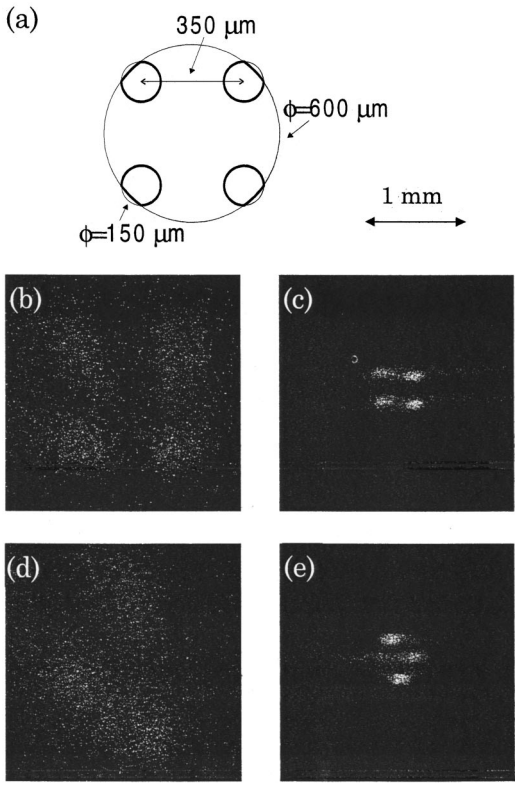

FIG. 3. (a) The object. (b) An image of the object shown in (a) when no voltages are applied. (c) An image when voltages $V_1 = V_3 = \pm 5.34$ kV and $V_2 = \pm 5.36$ kV are applied to each electrode. (d) An image of the rotated object when no voltages are applied. (e) An image of the rotated object when the same voltages as in (c) are applied.

where the suffices 1, 2, and 3 denote the first, second, and third lenses, respectively, and t_a, t_b, t_c, and t_d are the transit time in the gaps between two optical components from the object to the screen. The drift matrix M that describe the motion of atoms between two optical components is given by

$$M(t) = \begin{pmatrix} 1 & t \\ 0 & 1 \end{pmatrix},$$

where t is the transit time of the atom. The conditions to produce the inverted perfect image of the 1:1 magnification ratio are $(M_x)_{11} = (M_y)_{11} = -1$ and $(M_x)_{12} = (M_y)_{12} = 0$, which can be satisfied by a proper choice of the characteristic frequencies and transit times.

The experimental setup is shown in Fig. 2. To generate a cold atomic beam a transfer laser at the $\lambda = 598$ nm was focused into the magneto-optical trap of Ne atoms in the $1s_5[(2p)^5 3s{:}^3P_2]$ state. Approximately a half of the atoms were transferred to the $1s_3(J=0)$ state and fell vertically, pulled by gravity. All optical components were aligned vertically. The atom passed through the object that was located 172.5 mm below the trap, moved through the three lenses, and hit the microchannel plate detector that was placed 1003 mm below the trap. The object was composed of four holes that were symmetrically placed around the optical axis, whose detailed shape is shown in Fig. 3(a). The radius of the

cylinder was 24 mm, and the center of the two cylinder was separated by 56 mm, producing a minimum gap distance of 8 mm. The length of the three sets of cylinders and their separations were determined so that they formed a symmetric lens system along the $\pm z$ directions. Therefore, $T_1=T_3$, $t_a=t_d$, and $t_b=t_c$, which resulted in the image of the unit magnification. The ratio t_a/t_b was chosen to produce the correct image with the same characteristic frequency, $\omega_1=\omega_2=\omega_3=\omega$, for all three pairs when the identical voltage $\pm V$ was applied. The geometrical values that were used in the experiment are shown in Fig. 2. The fluorescent spots of individual atoms that hit the MCP were detected by a charge-coupled-device (CCD) camera and were recorded on a videotape. The data of their positions were retrieved through a videoprocessor, and the image was reconstructed by a personal computer.

When the electric potential is applied on only one of three lenses, the lens functions as a one-dimensional focusing lens. Since the size of the atomic source is finite, the image consists of four elongated ellipses around the focusing distance. The dimension that is listed in Fig. 2 gives the magnification factor of the one-dimensional images as -1.86, -1, and -0.537 for the three lenses, respectively. The electric potentials on the cylinder at which the distance of the ellipses along the convergent axis become equal to those magnifications were found to be $V_1=4.05$ kV, $V_2=3.15$ kV, and $V_3=3.95$ kV for the first, second, and third lenses, respectively. We used those voltages to derive the electric polarizability of the neon atom in the $1s_3$ state α. It was $2.8(\pm 0.1)\times 10^{-39}$ Fm^2. To our knowledge the electric polarizability of Ne has not been measured for the singlet metastable state $1s_3$. Shimizu *et al.* [17] gave a crude value of 10^{-39} Fm^2, which was estimated from the phase shift of an interferometric measurement. The present value is more than three times larger and is closer to the value obtained by Pritchard [18]. The electric potential to produce the correct image on the MCP with all three lenses was calculated by using the above values of the focusing potential for the single lens. It was $V=4.8$ kV. To find the best imaging condition experimentally the electric potential on each electrode was independently adjusted around this value. The potential to produce the best image was approximately 10% larger than the predicted value. As will be shown later, this result was mainly due to the edge effect that had been neglected. Figures 3(a) to 3(e) show experimentally obtained images. The horizontal and vertical sides of the figure coincide approximately to the x and y axes, respectively. Figure 3(b) is the atomic image when the electric potentials of all cylinders were zero. The large vague spots resulted from the projected pattern of the atomic cloud in the MOT through the hole of the object. Figure 3(c) is the image when the potential was $V_1=V_3=5.34$ kV and $V_2=5.36$ kV. In Figs. 3(d) and 3(e) the object was rotated approximately 55° and one of the four holes was blocked to verify experimentally that the image was inverted. Figure 4 shows the intensity profile of the image in Fig. 3(c) along the x and y axes. The distance between the image of two holes is approximately 300 μm. The image does not resolve the detailed shape of the hole. The diameter of the image of the hole at the half maximum point was 170 μm

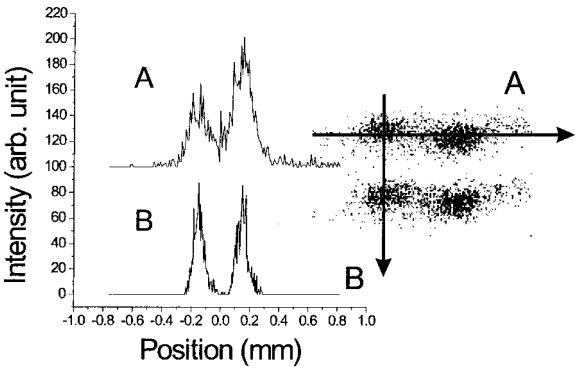

FIG. 4. Intensity profiles of the image [Fig. 3(c)] for the x and y axes.

along the x axis and 84 μm along the y axis. An extended tail was also observed along the x direction. The tail was mainly the result of the aberration arising from the higher-order terms of Eq. (1). Since the atom passes the second lens at a larger distance from the optical axis in the x-z plane, the effect of the aberration is larger along the x axis. The relatively poor imaging characteristics can be improved by using a more sophisticated shape for the electrode. Theoretically the aberration can be reduced to any value simply by increasing the radius R of the cylindrical electrode while keeping the distance d constant. In this case the electric potential of the electrode has to be increased approximately proportional to $\sqrt{R}$. Assuming that the shape of the atomic source was Gaussian, we estimated the effect of the missing edges of the holes in the object. The distance between the centers of the holes on the object to produce the observed pattern was 330 μm. Therefore, the magnification factor in Figs. 3(c) and 3(e) was 0.91.

In addition to the larger operating voltages, as mentioned above, the magnification factor of less than unit is also mainly the result of the edge effect of the two-cylinder lens. The three-dimensional electric potential is given to the third order of the power series on x and y [15] by

$$V(x,y,z)=U(z)x+\left(W(z)-\frac{U(z)''}{6}\right)x^3-3W(z)xy^2,$$

where $U(z)$ is the magnitude of the electric field on the optical axis, and $W(z)$ is a function that varies with the geometry of the electrode. This gives the z-dependent spring constant for the x and y axes,

$$k_x(z)=-\alpha U(6W-U'')^2-\alpha(U')^2,$$
$$k_y(z)=6\alpha UW, \tag{4}$$

which have different magnitudes near the edge. The shape of the $k_x(z)$ and $k_y(z)$ changes depending on the shape of the electrode. The approximate functional shapes in the present electrode geometry are shown in Fig. 1(b), which were calculated by assuming that d was much smaller than R and the length of the cylinder. The spring constant k_x along the divergent axis shoots up to the edge, while the k_y along the convergent axis decreases smoothly to zero. The edge effect

is, therefore, relatively small among the convergent axis, but increases the divergent angle along the divergent axis. We may approximate this effect on the transfer matrix M_d by replacing ω in Eq. (2) by $\gamma\omega$ with $\gamma>1$. This results in the higher operating voltages of the triplet lenses. The γ of three lenses that are calculated from the dimensions shown in Fig. 2 are $\gamma_1=1.22$, $\gamma_2=1.14$, and $\gamma_3=1.17$ for the first, second, and third lenses, respectively. Those values can be obtained experimentally by measuring the separation of the ellipses along the divergent axis in the one-dimensional image as a function of the applied voltage. They were $\gamma_1=1.30$, $\gamma_2=1.27$, and $\gamma_3=1.25$. The γ values are influenced also by the environment of the electrode. In this calculation the ground potential is assumed to be at an infinite distance. When the ground is brought near the electrode, the γ values increase. This can elucidate the larger experimental γ values because there exist complicated grounded metals near the electrodes in the real experiment. The difference of the characteristic frequency along the two axes changes the magnification factor of the three lens system. The latter experimental value of γ gives theoretically the magnification factor of 0.95, which agrees qualitatively with the experiment. To make the quantitative comparison with experiment a more accurate model of the electrode configuration, the misalignment of the lens system, as well as the higher-order terms of the interaction potential have to be taken into consideration. A detailed discussion of the imaging characteristics of the three two-cylinder lens system will be given in a separate paper.

In conclusion we have demonstrated two-dimensional imaging of a neutral atomic beam by a static electric field. The atomic image of a simple object with a 1:1 magnification ratio was obtained using a system that was composed of three electrostatic concave-convex lenses. Different magnifications can be obtained by changing the focal distance of each lens. A relatively large astigmatism and small interaction energy are the obstacles to obtaining a large aperture lens with high quality. However, the electric lens can be used for atoms with zero angular momentum. In addition, since the electric field can be controlled very accurately this lens system provides a new technique for the precise control of atomic motion. The electric polarizability of the $1s_3$ neon atom was determined as a by-product of this research.

This work has been partly supported by the Grants in Aid for Scientific Research (11216202) from the Ministry of Education, Science, Sports and Culture. This work was initiated by M. Morinaga, who suggested the imaging with two electrostatic lenses. We are also grateful to Y. Kurita for help in the experiment.

[1] C. S. Adams, M. Sigel, and J. Mlynek, Phys. Rep. **240**, 143 (1994).
[2] See, for example, N. F. Ramsey, *Molecular Beams* (Oxford University Press, New York, 1956).
[3] W. G. Kaenders *et al.*, Nature (London) **375**, 214 (1995); W. G. Kaenders *et al.*, Phys. Rev. A **54**, 5067 (1996).
[4] O. Carnal *et al.*, Phys. Rev. Lett. **67**, 3231 (1991).
[5] M. Morinaga *et al.*, Phys. Rev. Lett. **77**, 802 (1996).
[6] J. P. Gordon, Phys. Rev. **99**, 1253 (1955).
[7] W. Ketterle and D. E. Pritchard, Appl. Phys. B: Photophys. Laser Chem. **54**, 403 (1992).
[8] G. Timp *et al.*, Phys. Rev. Lett. **69**, 1636 (1992).
[9] J. E. Bjorkholm *et al.*, Phys. Rev. Lett. **41**, 1361 (1978).
[10] V. I. Balykin and V. S. Letokhov, Opt. Commun. **64**, 151 (1987).
[11] T. Sleator *et al.*, Appl. Phys. B: Photophys. Laser Chem. **54**, 375 (1992).
[12] P. Lemonde *et al.*, Europhys. Lett. **32**, 555 (1995).
[13] K. Shimizu *et al.*, in *Laser Spectroscopy, XII International Conference*, edited by M. Inguscio, M. Allegrini, and A. Sasso (World Scientific, Singapore, 1996), p. 140.
[14] R. J. C. Spreeuw *et al.*, Phys. Rev. Lett. **72**, 3162 (1994).
[15] M. Szilagyi, *Electron and Ion Optics* (Plenum Press, New York, 1988).
[16] A. Septier, *Advances in Electronics and Electron Physics*, edited by L. Marton (Academic, New York, 1961), Vol. XIV, pp. 85–205.
[17] F. Shimizu, K. Shimizu, and H. Takuma, Proc. SPIE **1726**, 193 (1992); F. Shimizu, in *Atomic Physics 13*, edited by H. Walther, T. Hänsch, and B. Neizert, AIP Conf. Proc. No. 275 (AIP, New York, 1993).
[18] C. R. Ekstrom *et al.*, Phys. Rev. A **51**, 3883 (1995).